Computation of the thermal expansion coefficient of graphene with Gaussian approximation potentials

Computation of Thermal Expansion Coefficient of Graphene with Gaussian Approximation Potentials

İlker Demiroğlu[a*], Yenal Karaaslan[b], Tuğbey Kocabaş[c], Murat Keçeli[d], Álvaro Vázquez-Mayagoitia[d], and Cem Sevik[b,e*]

[a] Department of Advanced Technologies, Eskisehir Technical University, Eskisehir, TR 26555, Turkey.

[b] Department of Mechanical Engineering, Eskişehir Technical University, Eskisehir, TR 26555, Turkey.

[c] Department of Materials Science and Engineering, Institute of Graduate Programs, Eskişehir Technical University, Eskisehir, TR 26555, Turkey.

[d] Computational Science Division, Argonne National Laboratory, Lemont, IL 60439, USA.

[e] Department of Physics, University of Antwerp, Groenenborgerlaan 171, 2020 Antwerp, Belgium

[*] E-mails: ilkerdemiroglu@eskisehir.edu.tr, csevik@eskisehir.edu.tr

Abstract

Direct experimental measurement of thermal expansion coefficient without substrate effects is a challenging task for 2D materials and its accurate estimation with large-scale *ab initio* molecular dynamics is computationally very expensive. Machine learning based interatomic potentials trained with *ab initio* data have been successfully used in molecular dynamics simulations to decrease the computational cost without compromising the accuracy. In this study, we investigated using Gaussian Approximation Potentials to reproduce the density functional theory level accuracy for graphene within both lattice dynamical and molecular dynamical methods, and to extend their applicability to larger length and time scales. Two such potentials are considered, GAP17 and GAP20. GAP17, which was trained with pristine graphene structures, is found to give closer results to density functional theory calculations at different scales. Further vibrational and structural analysis verify that the same conclusions can be deduced with density functional theory level in terms of the reasoning of the thermal expansion behavior and the negative thermal expansion behavior is associated with the long range out of plane phonon vibrations. Thus, it is argued that the enabled larger system sizes by machine learning potentials may even enhance the accuracy compared to small size limited *ab initio* molecular dynamics.

Keywords: negative thermal expansion, molecular dynamics, quasi-harmonic approximation, Grüneisen parameters, density functional theory, graphene, machine learning, gaussian approximation potential, acoustic phonons, rippling

Introduction

Graphene, a monolayer structure having a single-layer of sp^2 hybridized carbon atoms, has attracted the attention of both academia and industry since its successful isolation,[1] thanks to its fascinating physical properties[2–4] and rich potential for application to next-generation device technologies[5–7]. The thermal expansion coefficient (TEC) of graphene is one of the most important thermodynamic characteristics in determining the performance of graphene-based devices and in modulating the electronic properties of graphene. Unfortunately, experimental[8–15] and theoretical[16,17,26,18–25] studies have reported diverse results such as all-negative[9,10,13,15–18,26], all-positive[11,24–26], or sign-changing[8,12,26,14,19–25] variations regarding the TEC of graphene. The variety in these results is generally attributed to the insufficient representation of the anharmonicity for theoretical studies,[27–29] which is especially strong for two-dimensional crystals[23]. On the other hand, the unwanted substrate effects and the transparency of 2D materials makes conventional optical approaches difficult for the experimental studies.[30]

The first experimental TEC measurement of graphene was carried out by Bao et al.[8] using the scanning electronic microscopy. They found that the graphene's TEC has a negative value at low temperatures (with a room temperature value of -7×10^{-6} K^{-1}) and a sign change to positive at around $350K$ for temperatures between 300 K and 400 K. Yoon et al.[10] measured a negative TEC for all temperature range ($200 - 400$ K) with a room temperature value of $(-8 \pm 0.7) \times 10^{-6}$ K^{-1} using Raman spectroscopy. However, Linas et al.[11] reported all positive TEC values above room temperature by using Raman scattering measurements for graphene deposited on silicon nitride substrates in the temperature range $150 - 800$ K. On the theoretical side, using first-principles based on the density-functional perturbation theory and quasi-harmonic approximation simulations, Mounet and Marzari[16] reported that the TEC of graphene is negative up to 2500 K and is around -3.6×10^{-6} K^{-1} as approximately two times smaller than the experimental measurements at room temperature. With analytical and numerical lattice dynamical methods, Michel et al.[20] found that the transition temperature of the change from negative to positive TEC is lowered and close to 300 K for systems of macroscopic size, as a consequence of the corresponding change of the dispersion of the flexural mode at long wavelengths. Furthermore, Sevik[17], Kim et al.[18], and Mann et al.[19] reported similar results as [19] obtained by using quasi-harmonic approximation (QHA). In addition to these vibrational studies, classical molecular dynamics simulations that uses empirically parameterized inter-atomic potentials, which allow large system sizes, are also used to determine the TEC of graphene[23–26]. For example, in calculations made using atomistic Monte Carlo simulations by Zakharchenko et al.[23], the TEC of graphene exhibit a crossover from negative to positive at near 900 K and the average value to be -4.8×10^{-6} K^{-1}between the temperature ranges $0 - 300$ K. Moreover, using Monte Carlo simulations, Magnin et al.[26] carried out the MD calculations with several potentials covering empirical to semiempirical bond-order types, as well as a model based on tight-binding theory. However, they reported that the TEC resulting from these variations remain positive below 2000 K, unlike existing experimental measurements[8–11]. That is probably because the empirical inter-atomic potentials are not usually sufficiently accurate and transferable to describe other physical properties of the material in question simultaneously other than the property they were built-in for. More accurate calculations need quantum mechanical description in MD simulations, however, these types of calculations are computationally very demanding and limited by reduced system sizes.

Nowadays, it is claimed that the interatomic interactions can be defined with high accuracy thanks to the machine learning potentials such as Neural Network Potentials[31], Gaussian Approximation Potential (GAP)[32], Spectral Neighbor Analysis Potential[33], Moment Tensor Potentials[34]. Consequently, more accurate results can be obtained theoretically for the properties of the materials, such as TEC, which usually requires simulating large system sizes. For the last few years, different working groups have started developing machine learning potentials for graphene[35–41]. However, it is still not clear whether these machine learning potentials could reach the accuracy required for thermal properties. In this context, we discuss the efficiency of one of the promising machine learning potentials developed for graphene by Rowe et al.[35] based on GAP method. This potential reproduces the accuracy of *ab initio* density functional theory (DFT) calculations better than the more recent GAP potential[36] trained to a variety of carbon structures. For this purpose, we conducted lattice dynamics and molecular dynamics calculations to estimate TEC of graphene.

Methods

In this article, we estimate the TEC of graphene by three different methods: I) Quasi harmonic approximation (QHA) by minimizing Helmholtz energies at corresponding temperatures, II) Grüneisen framework by calculating mode-dependent Grüneisen parameters, and III) molecular dynamic (MD) simulations by comparing the in-plane area on different temperature runs. All calculations were done with two GAP models for carbon (denoted GAP17 and GAP20) and PBE exchange-correlation DFT functional as their energy basis for comparison. The details of the GAP models were taken from the ref 35 (GAP17) and ref 36 (GAP20), and the parameter files of both models were obtained from http://www.libatoms.org website (visited in August 2020). For DFT calculations, Local density approximation[42] and projector augmented wave[43,44] methods are used together with 500 eV plane wave basis cutoff-energy within the Vienna ab initio simulation package (VASP)[45,46]. The PHONOPY code[47] is used extensively for the vibrational analysis together with in-house codes to further analysis and fitting. In the part of QHA and Grüneisen framework, 8×8×1 conventional supercell structure and 4×4×1 Γ centered *k*-points grid were considered. The MD simulations with GAP models were performed using the Large-scale Atomic/Molecular Massively Parallel Simulator (LAMMPS)[48,49], with 5×10^5 time steps ($time\ step = 0.5$ fs) in NPT ensemble. The first 50 ps was considered as the process of reaching the thermal equilibrium and the TEC calculations were carried out over the last 200 ps. The MD simulations for graphene structures were performed in 3D box type simulation cells containing 448, 1008, 2232, 4032, and 6240 atoms, with widths approximately 3.4, 5.1, 7.6, 10.3, and 12.8 nm, respectively. In *z*-direction, 2 nm vacuum space is used to eliminate spurious periodic interactions. Isothermal-isobaric (NPT)[50,51] ensemble have been selected for *ab-initio* molecular dynamics[52,53] (MD) simulations as well. All *ab-initio* MD simulations lasted at least 8 ps with a time step of 1 fs. In all NPT MD simulations, $\vec{x}$ and $\vec{y}$ vectors are relaxed seperately while the $\vec{z}$ axis is kept fixed."

Results & Discussion

Calculated phonon dispersion relations given in Figure 1a shows that both GAP models match qualitatively well with the DFT. There is a good overlap of acoustic modes while the optic modes deviate slightly. Quantitatively, the average difference of the calculated phonon frequencies with DFT is 2.73 and 4.14 meV, while the maximum deviation from DFT is 8.05 meV and 13.03 meV for GAP17 and GAP20, respectively. According to these results, GAP17 predicts phonon frequencies closer to the DFT than GAP20. This relatively good match with DFT also holds for our calculations in compressed and strained supercells. The average difference with DFT for GAP17 (GAP20) is 2.78 meV (4.15 meV) when compressed by 1% and 2.74 meV (2.64 meV) when strained by 1%. Although in strained case the average differences for GAP20 is less than for GAP17, the maximum deviations are always larger for GAP20 case by around 3-4 meV. Similar to the DFT case, both GAP models also predict imaginary frequencies for ZA mode near to the Γ point of the Brillouin zone when the graphene is compressed (see Figure 1b). In general, the frequencies for the lowest energy mode (ZA) decreases with the compression and increases with the positive strain as in the DFT case. How the phonon frequencies change with respect to strain is important as they are used in the estimation of TEC by the QHA. However, negative phonon frequencies are a big problem here as they are not valid in QHA. Moreover, the acoustic phonons, especially the ZA mode, near the Γ point is known to be crucial in determining thermal properties of layered materials.[54] Thus, we fit the lowest energy frequencies (ZA mode) in the compressed cases by using the linear behavior of the strained cases. However, in general the behavior deviates from linearity with the increase in strain, thus limits our QHA approach within the linear regime (up to ±1.5% strain). We checked the validity of fitting the vibrational frequencies by comparing all the modes reproduced (dashed lines in Figure 1b) to the original ones and apart from the imaginary frequencies close to the Γ point in ZA mode, all other phonon frequencies are reproduced with relatively good accuracy with linear fitting up to −1.5% strain and more deviations starts thereafter (see Supplementary Figure S1).

Alternative to the QHA, Grüneisen framework can be used as well to estimate TEC. Mode Grüneisen parameters ($\gamma_{q,j}$),which are often used as a heuristic method to quantify anharmonicity, basically are the strain dependence of phonon frequencies:

$$\gamma_{q,j} = \frac{-a_0}{\omega_{q,j}} \frac{\partial \omega_{q,j}}{\partial a}$$

where a_0 is the unit cell constant, $\omega_{q,j}$ is the vibrational frequency corresponding to wave vector q and mode j. Within Grüneisen framework, TEC (α) can be estimated by using mode-dependent Grüneisen parameters via the mean Grüneisen parameter (γ_{mean}) as:

$$\alpha = \frac{\gamma_{mean} C^V}{B_T V_0}\Bigg|_{a,T}$$

where $c_{q,j}$ is the mode specific heat, C^V is the heat capacity, B_T is the bulk modulus and the (γ_{mean}) can be obtained from the mode-dependent Grüneisen parameters by:

$$\gamma_{mean} \equiv \frac{\sum_{q,j} \gamma_{q,j} c_{q,j}}{\sum_{q,j} c_{q,j}}$$

Mode Grüneisen parameters calculated over a 100 × 100 q-mesh are given in Figure 2 for both GAP models and DFT. Apart from the small deviations for TA and LA acoustic branches around Γ point, GAP17 model reproduces the mode Grüneisen parameters very accurately from the DFT. In general, the ZA branch (the out of plane vibration) is the main negative contributor while the optic branches are condensed slightly above 0 for both GAP17 model and DFT. On the other hand, GAP20 model overestimates the negative contributions of TA and LA modes.

The calculated TEC curves between 50-600 K are given in Figure 3. For GAP17 model the TEC curves obtained from Grüneisen framework and QHA are very close, while there is larger difference between them for DFT and GAP20 model. For GAP17 model, the lowest TEC values are obtained at around 220 K as -5.88×10^{-6} K^{-1} and -5.63×10^{-6} K^{-1}, while the values increase to -5.61×10^{-6} K^{-1} and -5.42×10^{-6} K^{-1} at room temperature for QHA and Grüneisen framework, respectively. When compared to DFT the behavior of TEC is almost the same while the values for GAP17 model are slightly higher (less negative thermal expansion) for both QHA and Grüneisen framework. The lowest TEC values are obtained at 240 K in the DFT case. The difference to GAP17 model is found to be higher for the QHA than Grüneisen, which is attributed to the nonlinear behavior of phonon frequencies are not as well represented in GAP17 model for the highly strained cases (1% - 1.5%) as it is trained mainly around to the optimized graphene monolayer and thus it is more accurate close to the ground state graphene. On the other hand, GAP20 model, which is trained to a variety of carbon structures, overestimate the TEC for QHA and Grüneisen framework by a large margin.

As a last method to estimate TEC, we used MD simulations with both GAP models and compared it to DFT. In this part of the study, we focused more on GAP17 model as it reproduces DFT with better accuracy due to more specialized training parameters; GAP17 was produced with graphene structures. Moreover, the MD and the lattice dynamics TEC results are inconsistent for GAP20 model while they are more consistent for GAP17 model (see Figure 3c and 3d). For example, when we compare the average TEC differences between the values from 6240 atom MD simulations and from the QHA calculations, there is 0.84×10^{-6} K^{-1} difference for GAP17 while there is 4.32×10^{-6} K^{-1} for GAP20 in the considered 50-600 K temperature range. In MD simulations, we tracked the in-plane area of graphene monolayer and through evaluation of the system with temperature we observed that the in-plane area is decreasing with the increasing temperature, which is the basis of the negative thermal expansion behavior. The in-plane area values are calculated as the area between the unit cell vectors $\vec{x}$ and $\vec{y}$ and then averaged over the simulation time (see Supplementary Figure S2 for the example fluctuations of $\vec{x}$ and $\vec{y}$). The area values are then used to calculate the TEC after fitting to cubic splines to smooth out the noise coming from single temperature runs:

$$\alpha = \frac{1}{A(T)} \frac{dA(T)}{dT}$$

where $A(T)$ is the smoothed Area under temperature T. To allow the comparison of different supercell sizes the Normalized Area values ($A/A0$, where $A0$ is the in plane area of relaxed system) are given in Figure 3a and 3b which shows the in-plane contraction with the increasing temperature. The degree of the contraction is lower for the smaller supercell as it constrains the larger in-plane vibrations but should converge with the increasing supercell size. Here, the system size is raised up to 6240 atoms to ensure the convergence. Keep in mind that

these system sizes are almost impossible for DFT calculations. We performed DFT MD calculations within our computational limits up to 448 atoms.

In general, the MD method is expected to be more accurate than lattice dynamics methods in TEC estimation as it incorporates full anharmonic interactions. However, the system size becomes here as a bottleneck, which may constrain the long wavelength out of plane oscillations. When we compare the TEC obtained from GAP17 model MD (6240 atom) to DFT, we see a decrease in the thermal expansion behavior, which the extent is probably missed by the smaller sized DFT supercells (see Figure 3c). Furthermore, when we compare the TEC obtained from MD simulations (-4.5×10^{-6} K^{-1} at RT), it is slightly lower in magnitude than obtained from lattice dynamics methods (~ -5.5×10^{-6} K^{-1} at RT). Altogether, these values are slightly lower in magnitude than the experimental values reported by Bao et al. (-7×10^{-6} K^{-1} at RT)[8] and Yoon et al. (-8×10^{-6} K^{-1} at RT)[10], however, those values are consistent with another recent experimental study of Pan et al. (-5.5×10^{-6} K^{-1} at RT)[15] which discards the substrate effect. We assume that it is quite probable in the former experimental studies that the TEC becomes positive quite rapidly at around 400 K due to the substrate effects as other experimental and theoretical studies in general confirm a more moderate increase in the TEC with a lower slope around RT.[9,15–17,23]

The MD simulations also allow a closer inspection on the structural origin of the thermal contraction by statistical analysis such as radial distribution function and variance in atomic coordinates. Especially the z-axis variance on the coordinates can give a statistical picture of the rippling behavior (see Figure 4a) of the graphene monolayers. The radial distribution analysis shows that the C-C bond lengths increase with the temperature (see Figure 4b) contrary to the expected decrease for a contraction behavior. Moreover, both GAP17 model and DFT MD simulations predict the same C-C bond length versus temperature trend regardless of the system size (see Figure 4c). On the other hand, the variance in z-axis coordinates of the carbon atoms increases with the temperature, which results in a decrease in the in-plane area of the graphene monolayer despite the increasing C-C bond lengths. In a lattice dynamical perspective, this rippling behavior is the outcome of the excitations of out of plane phonon vibrations, in particular ZA mode. This is also consistent with the differences in the extent of the rippling behavior changing with the system size, i.e. the smaller unit cell sizes hinder the long wavelength excitations. Thus, the GAP17 model may even improve the accuracy in MD simulations as it allows much larger system sizes than DFT without compromising the accuracy. However, it should be also noted that the same size GAP17 MD calculation (448-atom) underestimates the TEC compared to DFT which hints the lower accuracy of GAP17 at low system sizes.

The main advantage of ML based interatomic potentials is the reduced computational time compared to *ab initio* MD simulations. Table 1 summarizes the average computational times taken in our computer system both for DFT and GAP models MD simulations on the same computer architecture (Intel Xeon CPU E5-2680 v4 2.40 GHz, 128GB memory). Keep in mind that the system sizes are already different and ~1000 atoms are out of reach for DFT MD simulations in our systems as the limiting computational resources are not only time but also memory and the processing power. Starting with the 240-atom size DFT MD simulations, we needed to use multiple CPU nodes to meet the memory requirements. Moreover, simulation lengths are also order of magnitude different: in DFT we were limited by 10000 steps (10 ps) while 500000 steps (0.25 ns) are used in GAP model MD simulations. For GAP models, simulation times increase linearly with the increasing system size, however for DFT, simulation times expand quite rapidly despite using a greater number of CPUs. We also note that computational time scales linearly with the system size for the GAP calculations, while it scales cubically for the DFT calculations.

Conclusions

In summary, in this study we investigated the accuracy of the machine learning GAP models in the TEC estimation of graphene. The one-to-one comparison of phonon frequencies hint that the GAP models catches the lattice dynamics of graphene very well, especially with GAP17 model. Thus, the TEC estimation from the Grüneisen framework is the closest to the DFT calculated value. On the other hand, there are larger differences in QHA due to the non-linear behavior of the vibrational frequencies at the limits in the selected strain range. The molecular dynamical simulations show that GAP17 model captures the origin of the thermal expansion similar to the DFT level calculations. The negative thermal expansion is associated with the rippling behavior caused by the out of plane vibrations (ZA mode) as the C-C bond lengths increase with the increasing temperature.

Acknowledgements

Computational resources were provided by the High Performance and Grid Computing Center (TRGrid e-Infrastructure) of TUBITAK ULAKBIM and the National Center for High Performance Computing (UHeM) of Istanbul Technical University. We gratefully acknowledge the computing resources provided on Bebop, a high-performance computing cluster operated by the Laboratory Computing Resource Center at Argonne National Laboratory and resources at Argonne Leadership Computing Facility, which is a DOE Office of Science User Facility supported under Contract DE-AC02-06CH11357. MK is supported by Laboratory Directed Research and Development (LDRD) funding from Argonne National Laboratory, provided by the Director, Office of Science, of the U.S. Department of Energy under Contract No. DE-AC02-06CH11357. ID and CS acknowledge the support from the Eskisehir Technical University (ESTU-BAP 20ADP210 and 20ADP246). TK would like to thank to the Scientific and Technological Research Council of Turkey (TÜBİTAK BİDEB 2211) and Council of Higher Education of Turkey (YÖK 100/2000) for doctoral scholarship.

Supporting Information

All the calculated phonon frequencies versus applied strain. The variation in length of x and y vectors during MD simulations.

Corresponding Authors

İlker Demiroğlu and Cem Sevik

* Emails: ilkerdemiroglu@eskisehir.edu.tr, csevik@eskisehir.edu.tr

Author Contributions

The manuscript was written through contributions of all authors. All authors have given approval to the final version of the manuscript.

Conflicts of Interest

None.

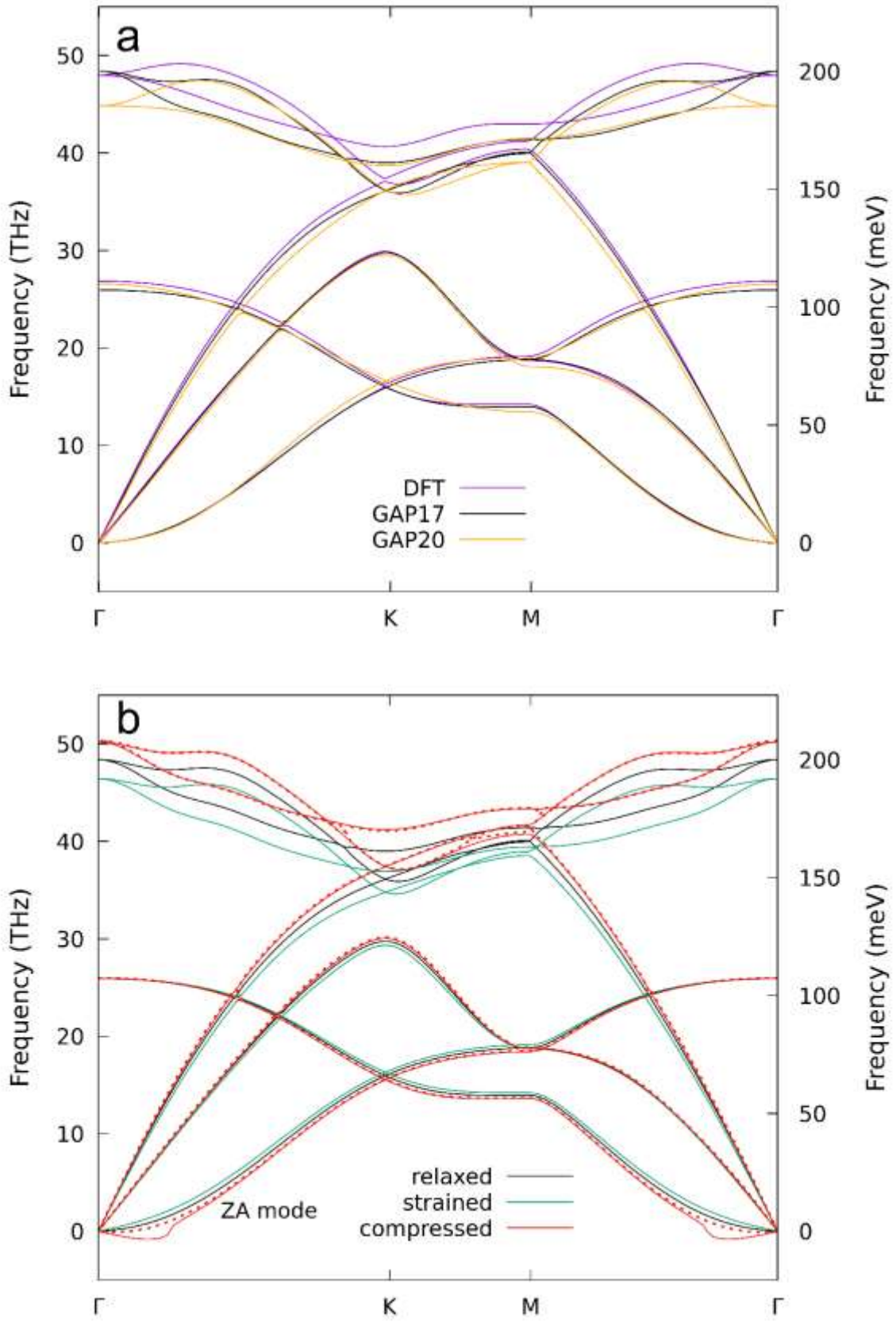

Figure 1. a) Phonon dispersion relations of relaxed graphene monolayers by DFT, GAP17 and GAP20 models. b) Phonon dispersion relations of relaxed, 1% strained and 1% compressed graphene monolayers by GAP17 model compared to DFT. Dashed line shows the corrected phonon curves of the compressed case.

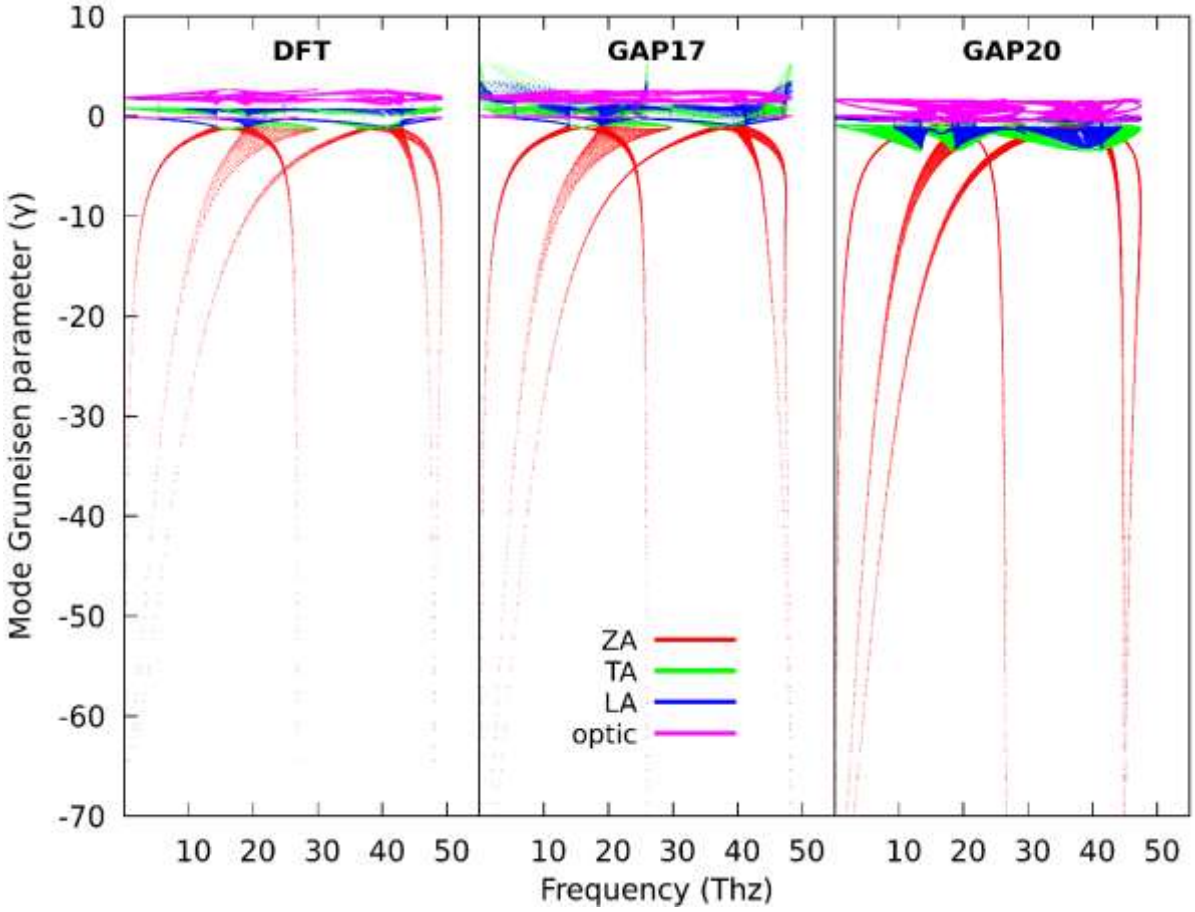

Figure 2. Calculated mode Grüneisen parameters for DFT, GAP17 and GAP20 models over a 100 × 100 q-mesh.

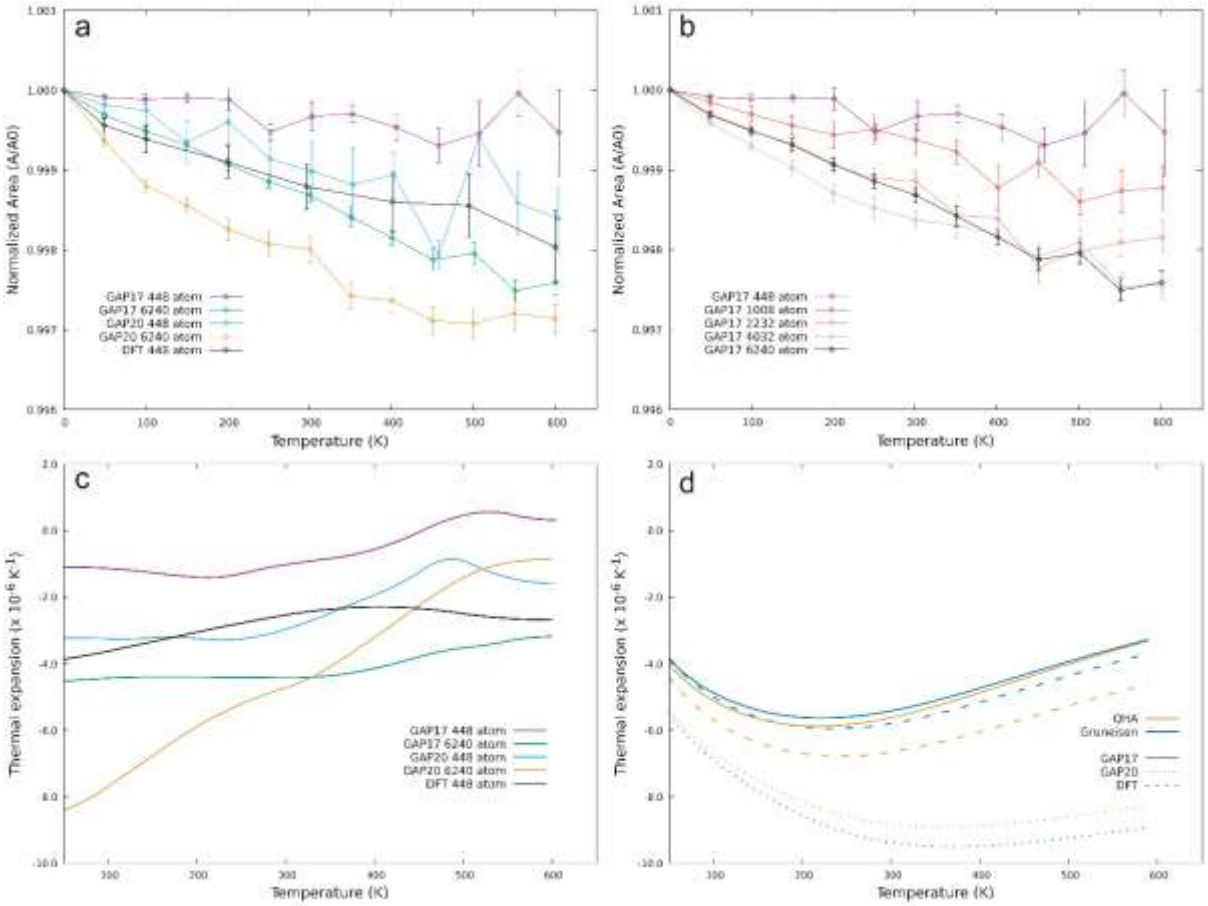

Figure 3. a) Normalized Area versus simulation temperature for molecular dynamics calculations with DFT, GAP17 and GAP20 models. b) Normalized Area versus simulation temperature for molecular dynamics calculations GAP17 model w.r.t system size. c) Calculated thermal expansion coefficients of graphene by MD simulations with DFT, GAP17 and GAP20 models. d) Calculated thermal expansion coefficients of graphene QHA and Grüneisen framework with GAP models and DFT.

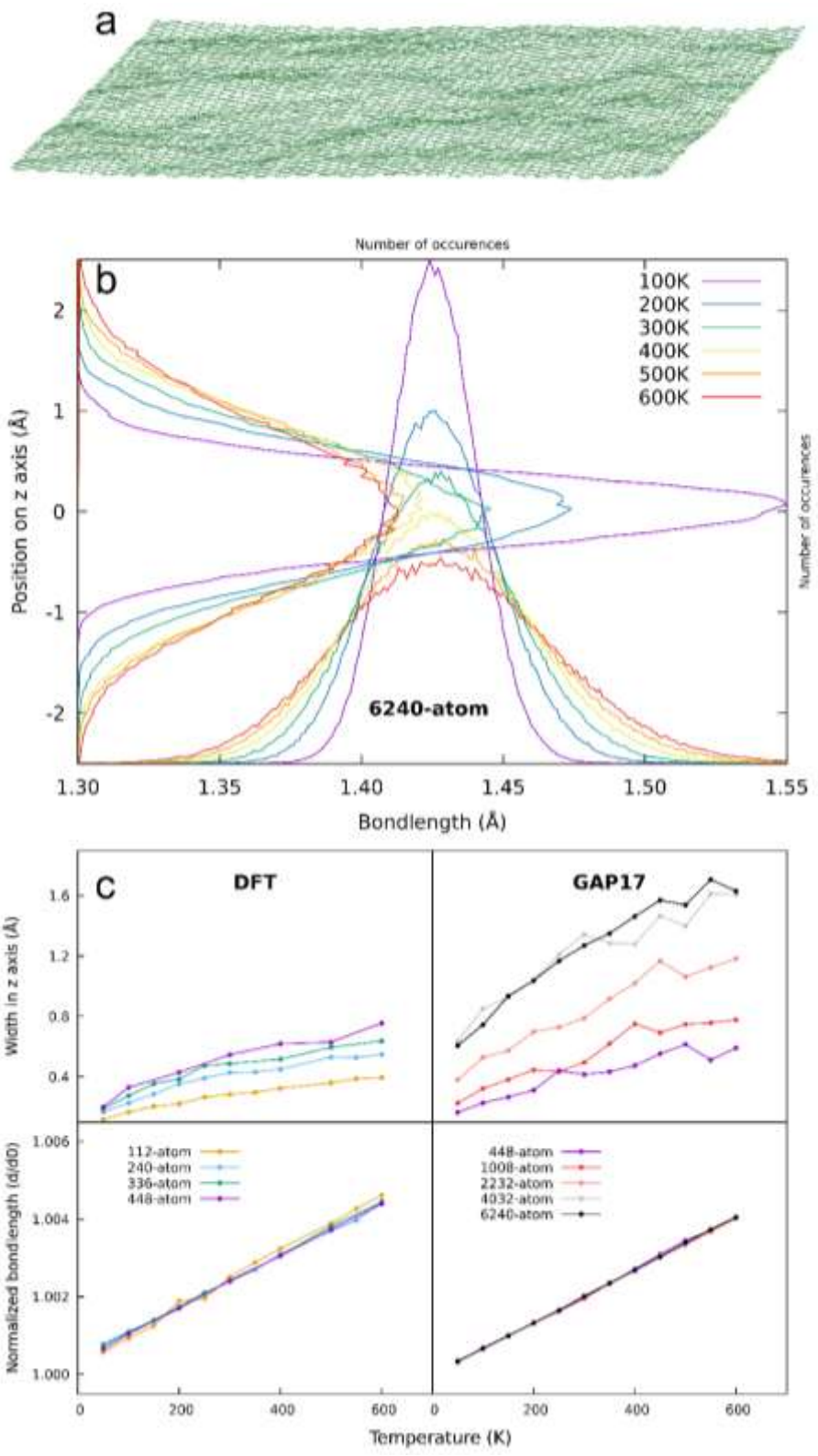

Figure 4. a) Side view of graphene monolayer within a MD frame demonstrating the rippling behavior. b) Structural analysis of 6240-atom graphene system obtained from MD simulations with GAP17 model. The bond length distribution is given in horizontal axis while the position distribution on *z*-axis is given in vertical axis against the number of occurrences. c) Normalized bond lengths versus temperature and rippling width versus temperature graphs of graphene obtained from MD simulations. Rippling width is calculated as 2σ from the standard deviation of the position distribution on z-axis and the bondlenghts are normalized by using the bondlength of the relaxed system (d0).

Table 1. Average simulation times for simulations performed with GAP models and DFT on the same computer architecture:

Method	System size	# of steps	# of CPU	Total time	Time per step
DFT	112-atom	10000	28 (1 node)	71 hours	26 s
DFT	240-atom	10000	56 (2 nodes)	170 hours	61 s
DFT	336-atom	10000	84 (3 nodes)	293 hours	106 s
DFT	448-atom	10000	112 (4 nodes)	574 hours	207 s
GAP	448-atom	500000	28 (1 node)	18 hours	0.2 s
GAP	1008-atom	500000	28 (1 node)	38 hours	0.4 s
GAP	2232-atom	500000	28 (1 node)	84 hours	0.7 s
GAP	4032-atom	500000	28 (1 node)	150 hours	1.1 s
GAP	6240-atom	500000	28 (1 node)	240 hours	1.7 s

References

(1) Novoselov, K. S.; Geim, A. K.; Morozov, S. V.; Jiang, D.; Zhang, Y.; Dubonos, S. V.; Grigorieva, I. V.; Firsov, A. A. Electric Field in Atomically Thin Carbon Films. *Science (80-.).* **2004**, *306* (5696), 666–669. https://doi.org/10.1126/science.1102896.

(2) Balandin, A. A.; Ghosh, S.; Bao, W.; Calizo, I.; Teweldebrhan, D.; Miao, F.; Lau, C. N. Superior Thermal Conductivity of Single-Layer Graphene. *Nano Lett.* **2008**, *8* (3), 902–907. https://doi.org/10.1021/nl0731872.

(3) Castro Neto, A. H.; Guinea, F.; Peres, N. M. R.; Novoselov, K. S.; Geim, A. K. The Electronic Properties of Graphene. *Rev. Mod. Phys.* **2009**, *81* (1), 109–162. https://doi.org/10.1103/RevModPhys.81.109.

(4) Ferrari, A. C.; Basko, D. M. Raman Spectroscopy as a Versatile Tool for Studying the Properties of Graphene. *Nature Nanotechnology*. Nature Publishing Group 2013, pp 235–246. https://doi.org/10.1038/nnano.2013.46.

(5) Huang, Y.; Liang, J.; Chen, Y. An Overview of the Applications of Graphene-Based Materials in Supercapacitors. *Small*. John Wiley & Sons, Ltd June 2012, pp 1805–1834. https://doi.org/10.1002/smll.201102635.

(6) Bae, S.; Kim, S. J.; Shin, D.; Ahn, J.-H.; Hong, B. H. Towards Industrial Applications of Graphene Electrodes. *Phys. Scr* **2012**, *T146*, 014024. https://doi.org/10.1088/0031-8949.

(7) Liu, Q.; Zhang, X.; Abdalla, L. B.; Fazzio, A.; Zunger, A. Switching a Normal Insulator into a Topological Insulator via Electric Field with Application to Phosphorene. *Nano Lett.* **2015**, *15* (2), 1222–1228. https://doi.org/10.1021/nl5043769.

(8) Bao, W.; Miao, F.; Chen, Z.; Zhang, H.; Jang, W.; Dames, C.; Lau, C. N. Controlled Ripple Texturing of Suspended Graphene and Ultrathin Graphite Membranes. *Nat. Nanotechnol.* **2009**, *4* (9), 562–566. https://doi.org/10.1038/nnano.2009.191.

(9) Singh, V.; Sengupta, S.; Solanki, H. S.; Dhall, R.; Allain, A.; Dhara, S.; Pant, P.; Deshmukh, M. M. Probing Thermal Expansion of Graphene and Modal Dispersion at Low-Temperature Using Graphene Nanoelectromechanical Systems Resonators. *Nanotechnology* **2010**, *21* (16). https://doi.org/10.1088/0957-4484/21/16/165204.

(10) Yoon, D.; Son, Y. W.; Cheong, H. Negative Thermal Expansion Coefficient of Graphene Measured by Raman Spectroscopy. *Nano Lett.* **2011**, *11* (8), 3227–3231. https://doi.org/10.1021/nl201488g.

(11) Linas, S.; Magnin, Y.; Poinsot, B.; Boisron, O.; Förster, G. D.; Martinez, V.; Fulcrand, R.; Tournus, F.; Dupuis, V.; Rabilloud, F.; Bardotti, L.; Han, Z.; Kalita, D.; Bouchiat, V.; Calvo, F. Interplay between Raman Shift and Thermal Expansion in Graphene: Temperature-Dependent Measurements and Analysis of Substrate Corrections. *Phys. Rev. B - Condens. Matter Mater. Phys.* **2015**, *91* (7), 075426. https://doi.org/10.1103/PhysRevB.91.075426.

(12) Tian, S.; Yang, Y.; Liu, Z.; Wang, C.; Pan, R.; Gu, C.; Li, J. Temperature-Dependent Raman Investigation on Suspended Graphene: Contribution from Thermal Expansion Coefficient Mismatch between Graphene and Substrate. *Carbon N. Y.* **2016**, *104*, 27–32. https://doi.org/10.1016/j.carbon.2016.03.046.

(13) Shaina, P. R.; George, L.; Yadav, V.; Jaiswal, M. Estimating the Thermal Expansion Coefficient of Graphene: The Role of Graphene-Substrate Interactions. *J. Phys. Condens. Matter* **2016**, *28*, 085301. https://doi.org/10.1088/0953-8984/28/8/085301.

(14) Li, C.; Liu, Q.; Peng, X.; Fan, S. Measurement of Thermal Expansion Coefficient of Graphene Diaphragm Using Optical Fiber Fabry-Perot Interference. *Meas. Sci. Technol.* **2016**, *27* (7), 075102. https://doi.org/10.1088/0957-0233/27/7/075102.

(15) Pan, W.; Xiao, J.; Zhu, J.; Yu, C.; Zhang, G.; Ni, Z.; Watanabe, K.; Taniguchi, T.; Shi, Y.; Wang, X. Biaxial Compressive Strain Engineering in Graphene/Boron Nitride Heterostructures. *Sci. Rep.* **2012**, *2* (1), 1–6. https://doi.org/10.1038/srep00893.

(16) Mounet, N.; Marzari, N. First-Principles Determination of the Structural, Vibrational and Thermodynamic Properties of Diamond, Graphite, and Derivatives. *Phys. Rev. B - Condens. Matter Mater. Phys.* **2005**, *71* (20), 205214. https://doi.org/10.1103/PhysRevB.71.205214.

(17) Sevik, C. Assessment on Lattice Thermal Properties of Two-Dimensional Honeycomb Structures: Graphene,h-BN, h-MoS2, and h-MoSe2. *Phys. Rev. B* **2014**, *89* (3), 035422. https://doi.org/10.1103/PhysRevB.89.035422.

(18) Kim, C.-W. W.; Kang, S.-H. H.; Kwon, Y.-K. K. Rigid Unit Modes in Sp-Sp2 Hybridized Carbon Systems: Origin of Negative Thermal Expansion. *Phys. Rev. B - Condens. Matter Mater. Phys.* **2015**, *92* (24), 245434. https://doi.org/10.1103/PhysRevB.92.245434.

(19) Mann, S.; Kumar, R.; Jindal, V. K. Negative Thermal Expansion of Pure and Doped Graphene. *RSC Adv.* **2017**, *7* (36), 22378–22387.

(20) Michel, K. H.; Costamagna, S.; Peeters, F. M. Theory of Anharmonic Phonons in Two-Dimensional Crystals. *Phys. Rev. B - Condens. Matter Mater. Phys.* **2015**, *91* (13), 134302. https://doi.org/10.1103/PhysRevB.91.134302.

(21) Jiang, J.-W.; Wang, B.-S.; Wang, J.-S.; Park, H. S. A Review on the Flexural Mode of Graphene: Lattice Dynamics, Thermal Conduction, Thermal Expansion, Elasticity and Nanomechanical Resonance. *J. Phys. Condens. Matter* **2015**, *27* (8), 083001. https://doi.org/10.1088/0953-8984/27/8/083001.

(22) Da Silva, A. L. C.; Cândido, L.; Teixeira Rabelo, J. N.; Hai, G. Q.; Peeters, F. M. Anharmonic Effects on Thermodynamic Properties of a Graphene Monolayer. *EPL* **2014**, *107* (5), 56004. https://doi.org/10.1209/0295-5075/107/56004.

(23) Zakharchenko, K. V.; Katsnelson, M. I.; Fasolino, A. Finite Temperature Lattice Properties of Graphene beyond the Quasiharmonic Approximation. *Phys. Rev. Lett.* **2009**, *102* (4), 046808. https://doi.org/10.1103/PhysRevLett.102.046808.

(24) Ghasemi, H.; Rajabpour, A. A Novel Approach to Calculate Thermal Expansion of Graphene: Molecular Dynamics Study. *Eur. Phys. J. Plus 2017 1325* **2017**, *132* (5), 1–5. https://doi.org/10.1140/EPJP/I2017-11491-Y.

(25) Gao, W.; Huang, R. Thermomechanics of Monolayer Graphene: Rippling, Thermal Expansion and Elasticity. *J. Mech. Phys. Solids* **2014**, *66* (1), 42–58. https://doi.org/10.1016/j.jmps.2014.01.011.

(26) Magnin, Y.; Förster, G. D.; Rabilloud, F.; Calvo, F.; Zappelli, A.; Bichara, C. Thermal Expansion of Free-Standing Graphene: Benchmarking Semi-Empirical Potentials - IOPscience. *J. Phys. Condens. Matter* **2014**,

26 (18), 185401. https://doi.org/10.1088/0953-8984/26/18/185401.

(27) Cowley, R. A. Anharmonic Crystals. *Reports Prog. Phys.* **1968**, *31* (1), 123. https://doi.org/10.1088/0034-4885/31/1/303.

(28) Leibfried, G.; Ludwig, W. Theory of Anharmonic Effects in Crystals. *Solid State Phys. - Adv. Res. Appl.* **1961**, *12* (C), 275–444. https://doi.org/10.1016/S0081-1947(08)60656-6.

(29) Burmistrov, I. S.; Gornyi, I. V.; Kachorovskii, V. Y.; Katsnelson, M. I.; Mirlin, A. D. Quantum Elasticity of Graphene: Thermal Expansion Coefficient and Specific Heat. *Phys. Rev. B* **2016**, *94* (19), 195430. https://doi.org/10.1103/PhysRevB.94.195430.

(30) Zhang, L.; Lu, Z.; Song, Y.; Zhao, L.; Bhatia, B.; Bagnall, K. R.; Wang, E. N. Thermal Expansion Coefficient of Monolayer Molybdenum Disulfide Using Micro-Raman Spectroscopy. *Nano Lett.* **2019**, *19* (7), 4745–4751. https://doi.org/10.1021/acs.nanolett.9b01829.

(31) Behler, J.; Parrinello, M. Generalized Neural-Network Representation of High-Dimensional Potential-Energy Surfaces. *Phys. Rev. Lett.* **2007**, *98* (14), 146401. https://doi.org/10.1103/PhysRevLett.98.146401.

(32) Bartók, A. P.; Payne, M. C.; Kondor, R.; Csányi, G. Gaussian Approximation Potentials: The Accuracy of Quantum Mechanics, without the Electrons. *Phys. Rev. Lett.* **2010**, *104* (13), 136403. https://doi.org/10.1103/PhysRevLett.104.136403.

(33) Thompson, A. P.; Swiler, L. P.; Trott, C. R.; Foiles, S. M.; Tucker, G. J. Spectral Neighbor Analysis Method for Automated Generation of Quantum-Accurate Interatomic Potentials. *J. Comput. Phys.* **2015**, *285*, 316–330. https://doi.org/10.1016/j.jcp.2014.12.018.

(34) Shapeev, A. V. Moment Tensor Potentials: A Class of Systematically Improvable Interatomic Potentials. *Multiscale Model. Simul.* **2016**, *14* (3), 1153–1173. https://doi.org/10.1137/15M1054183.

(35) Rowe, P.; Csányi, G.; Alfè, D.; Michaelides, A. Development of a Machine Learning Potential for Graphene. *Phys. Rev. B* **2018**, *97* (5), 054303. https://doi.org/10.1103/PhysRevB.97.054303.

(36) Rowe, P.; Deringer, V. L.; Gasparotto, P.; Csányi, G.; Michaelides, A. An Accurate and Transferable Machine Learning Potential for Carbon. *J. Chem. Phys.* **2020**, *153* (3), 034702. https://doi.org/10.1063/5.0005084.

(37) Mortazavi, B.; Novikov, I. S.; Podryabinkin, E. V.; Roche, S.; Rabczuk, T.; Shapeev, A. V.; Zhuang, X. Exploring Phononic Properties of Two-Dimensional Materials Using Machine Learning Interatomic Potentials. *Appl. Mater. Today* **2020**, *20*, 100685. https://doi.org/10.1016/j.apmt.2020.100685.

(38) Wan, J.; Jiang, J. W.; Park, H. S. Machine Learning-Based Design of Porous Graphene with Low Thermal Conductivity. *Carbon N. Y.* **2020**, *157*, 262–269. https://doi.org/10.1016/j.carbon.2019.10.037.

(39) Lin, S.; Xu, H.; Wang, Y.; Zeng, X. C.; Chen, Z. Directly Predicting Limiting Potentials from Easily Obtainable Physical Properties of Graphene-Supported Single-Atom Electrocatalysts by Machine Learning. *J. Mater. Chem. A* **2020**, *8* (11), 5663–5670. https://doi.org/10.1039/c9ta13404b.

(40) Wen, M.; Tadmor, E. B. Hybrid Neural Network Potential for Multilayer Graphene. *Phys. Rev. B* **2019**, *100* (19), 195419. https://doi.org/10.1103/PhysRevB.100.195419.

(41) Mortazavi, B.; Podryabinkin, E. V.; Novikov, I. S.; Rabczuk, T.; Zhuang, X.; Shapeev, A. V. Accelerating First-Principles Estimation of Thermal Conductivity by Machine-Learning Interatomic Potentials: A MTP/ShengBTE Solution. *Comput. Phys. Commun.* **2021**, *258*, 107583. https://doi.org/10.1016/j.cpc.2020.107583.

(42) Perdew, J. P.; Zunger, A. Self-Interaction Correction to Density-Functional Approximations for Many-Electron Systems. *Phys. Rev. B* **1981**, *23* (10), 5048–5079. https://doi.org/10.1103/PhysRevB.23.5048.

(43) Kresse, G.; Joubert, D. From Ultrasoft Pseudopotentials to the Projector Augmented-Wave Method. *Phys. Rev. B* **1999**, *59* (3), 1758–1775. https://doi.org/10.1103/PhysRevB.59.1758.

(44) Blöchl, P. E. Projector Augmented-Wave Method. *Phys. Rev. B* **1994**, *50* (24), 17953–17979.

https://doi.org/10.1103/PhysRevB.50.17953.

(45) Kresse, G.; Hafner, J. Ab Initio Molecular Dynamics for Liquid Metals. *Phys. Rev. B* **1993**, *47* (1), 558–561. https://doi.org/10.1103/PhysRevB.47.558.

(46) Kresse, G.; Hafner, J. Ab Initio Molecular-Dynamics Simulation of the Liquid-Metalamorphous-Semiconductor Transition in Germanium. *Phys. Rev. B* **1994**, *49* (20), 14251–14269. https://doi.org/10.1103/PhysRevB.49.14251.

(47) Togo, A.; Oba, F.; Tanaka, I. First-Principles Calculations of the Ferroelastic Transition between Rutile-Type and CaCl 2 -Type SiO 2 at High Pressures. *Phys. Rev. B* **2008**, *78* (13), 134106. https://doi.org/10.1103/PhysRevB.78.134106.

(48) LAMMPS Molecular Dynamics Simulator.

(49) Plimpton, S. Fast Parallel Algorithms for Short-Range Molecular Dynamics. *J. Comput. Phys.* **1995**, *117* (1), 1–19. https://doi.org/10.1006/jcph.1995.1039.

(50) Hernández, E. Metric-Tensor Flexible-Cell Algorithm for Isothermal-Isobaric Molecular Dynamics Simulations. *J. Chem. Phys.* **2001**, *115* (22), 10282–10290. https://doi.org/10.1063/1.1416867.

(51) *Computer Simulation of Liquids: Second Edition - Michael P. Allen, Dominic J. Tildesley - Google Kitaplar*.

(52) Parrinello, M.; Rahman, A. Polymorphic Transitions in Single Crystals: A New Molecular Dynamics Method. *J. Appl. Phys.* **1981**, *52* (12), 7182–7190. https://doi.org/10.1063/1.328693.

(53) Parrinello, M.; Rahman, A. Crystal Structure and Pair Potentials: A Molecular-Dynamics Study. *Phys. Rev. Lett.* **1980**, *45* (14), 1196–1199. https://doi.org/10.1103/PhysRevLett.45.1196.

(54) Bonini, N.; Garg, J.; Marzari, N. Acoustic Phonon Lifetimes and Thermal Transport in Free-Standing and Strained Graphene. *Nano Lett.* **2012**, *12* (6), 2673–2678. https://doi.org/10.1021/nl202694m.

Table of Contens figure: